Local time-correlation approach for calculations of x-ray spectra

A. J. Lee, F. D. Vila, and J. J. Rehr
Department of Physics, University of Washington, Seattle, Washington 98195, USA
(Received 26 June 2012; published 7 September 2012)

We present a local time-correlation function method for real-time calculations of core level x-ray spectra (RTXS). The approach is implemented in a local orbital basis using a Crank-Nicolson time-evolution algorithm applied to an extension of the SIESTA code, together with projector augmented wave (PAW) atomic transition matrix elements. Our RTXS is formally equivalent to ΔSCF (Δ self consistent field) Fermi's golden rule calculations with a screened core-hole and an effective independent particle approximation. Illustrative calculations are presented for several molecular and condensed matter systems and found to be in good agreement with experiment. The method can also be advantageous compared to conventional frequency-space methods.

DOI: 10.1103/PhysRevB.86.115107 PACS number(s): 78.70.Dm, 78.20.Bh, 78.70.En

I. INTRODUCTION

We present an approach for real-time calculations of x-ray spectra (RTXS), including x-ray absorption (XAS) and emission (XES), based on local time-correlation functions. Formally such correlation functions form the starting point for the many-body theory of x-ray spectra, e.g., in the classic work of Nozières and De Dominicis (ND).[1] Calculations based on time-correlation functions can be advantageous both formally and for practical calculations of many physical properties.[2] They have recently been applied to problems ranging from nonlinear optical response[3] to thermal vibrations.[4] Nevertheless, x-ray spectra for deep core-levels have traditionally been calculated in frequency space using Fermi's golden rule.[5–8]

Calculations of time-dependent response have been of increasing interest, especially with the advent of high brightness pulsed x-ray sources.[9] One approach to such calculations is based on time-dependent density functional theory (TDDFT).[10,11] Real-space, real-time implementations of TDDFT have been developed for both linear and nonlinear optical responses.[3,10] However, these approaches are currently restricted to the UV-VIS range due to basis set limitations, the need for very short time steps to treat the x-ray regime and very long simulation times to account for the valence response. The many-body formulation based on time-dependent Green's functions is particularly useful, e.g., to describe the x-ray edge singularity.[1,12] However, calculations of XAS within the ND formalism require transient Green's functions and the response to the sudden creation and destruction of a core hole, for which a number of approaches have been proposed.[13–15] Nevertheless, edge-singularity effects are most important in metallic systems near threshold, and are typically suppressed due to lifetime and other broadening effects.

For the above reasons, we restrict our attention in this paper to the simpler, limiting case of x-ray response in the presence of a static, adiabatically screened core-hole. The extension to dynamical response will be reserved for a subsequent paper. This initial step is interesting in its own right, since it facilitates comparison with frequency-domain calculations and is often a good approximation for molecular and nonmetallic materials. In particular, this limiting case is equivalent to Fermi's golden rule within a ΔSCF approximation in an effective, independent particle picture. For XAS, this picture is referred to as the *final-state rule*.[16] Like Green's function approaches in frequency space,[17] the time-correlation function method is efficient, since it avoids the need for explicit sums over occupied or unoccupied states and depends only on local properties. Indeed, the approaches are similar and can be related via time-Fourier transforms. Our approach is implemented using a real-time extension of the SIESTA code[3] with a Crank-Nicolson time-evolution operator,[18] and projector augmented wave (PAW) transition matrix elements.[19] This implementation results in a practical and generally applicable code that builds in full-potential electronic structure and self-consistent core-hole screening. Moreover, for the systems investigated, the code yields results in as good or better agreement with experiment than conventional frequency-space methods.

II. FORMALISM

A. Time-correlation function

Assuming that the core- and valence-electron states can be treated as independent, factorizable subspaces, our starting point is an expression for the core-level XAS $\mu(\omega)$ in terms of a local time-correlation function $\langle\psi_+(0)|\psi_+(t)\rangle$ defined below,

$$\mu(\omega) = \frac{1}{\pi}\,\mathrm{Re}\int_0^\infty dt\, e^{i\omega t} G_c(t)\langle\psi_+(0)|\psi_+(t)\rangle. \qquad (1)$$

The time correlation function characterizes the response to x-ray excitation *via* an interaction Hamiltonian (e.g., the dipole interaction) from a given core-orbital $|c\rangle$ with energy ϵ_c. Here $G_c(t) = i\theta(t)\exp[i(\epsilon_c + i\Gamma)t]$ is the bare core-hole Green's function with core-hole lifetime Γ. The time-evolution of $|\psi_+(t)\rangle$ is governed by the single-particle equation of motion:[2]

$$i\frac{\partial|\psi_+\rangle}{\partial t} = \mathbf{H}'(t)|\psi_+(t)\rangle, \qquad (2)$$

where $\mathbf{H}'(t)$ is the dynamic, final-state one-electron Hamiltonian in the presence of a core-hole in level $|c\rangle$. Here and elsewhere below, we use atomic units $e = \hbar = m = 1$, and a prime denotes the presence of a core hole. For deep core states, the initial "seed state" $|\psi_+(0)\rangle$ created by the dipole interaction $d(x)\exp(i\omega t)$ in XAS is

$$|\psi_+(0)\rangle \equiv \mathcal{P}\,|\psi(0)\rangle = \mathcal{P}\,d(x)|c\rangle, \qquad (3)$$

which is localized with respect to the absorption site. Here, $\mathcal{P} = \mathbf{1} - \Sigma_k^{\mathrm{occ}}|k\rangle\langle k|$ is the projector onto the subspace of

unoccupied valence and continuum states $|k\rangle$, i.e., energy eigenstates of the ground-state Hamiltonian above the Fermi energy E_F. This projection reflects the fact that transitions to occupied states are excluded in the full many-body treatment of XAS. For an inhomogeneous system, one must also average over the chemical shifts for all core-state energy levels. A typical time correlation function for the dipole response for the C K-edge XES of benzene is shown in Fig. 4.

The projector $\mathcal{P}$ can be handled in several ways: (i) one way is to construct $\mathcal{P} = \mathbf{1} - \Sigma_k^{\rm occ}|k\rangle\langle k|$ explicitly from the initial occupied Kohn-Sham states $|k\rangle$. (ii) A simpler alternative is to start with an unprojected seed state $|\psi(0)\rangle = d|c\rangle$. With this latter choice the restriction to unoccupied states is added *ex post facto* through Fourier filtering and the introduction of an *ad hoc* factor $\theta(E - E_F)$ in Eq. (1), where $E = \omega + \epsilon_c$. In practice, the Fermi energy E_F is set at midgap between the occupied and unoccupied states. In this paper, we have generally used this alternative approach (ii). However, a potential drawback is that the seed state may contain rapidly oscillating energy states that require relatively short time steps to treat accurately.

X-ray emission spectra (XES) can be calculated similarly from the correlation function $\langle\psi_-(0)|\psi_-(t)\rangle$ and a time-evolution similar to that in Eq. (2) governed by the initial state Hamiltonian $\mathbf{H}(t)$ (i.e., the *initial state rule*). Here, the seed state is $|\psi_-(0)\rangle = \mathcal{P}_{\rm occ}|\psi(0)\rangle$ i.e., with the projector $\mathcal{P}$ replaced by the projector $\mathcal{P}_{\rm occ} = \Sigma_k^{\rm occ}|k\rangle\langle k|$ onto occupied states below E_F. Unless otherwise specified, we will focus below on the XAS case, with the understanding that the treatment for XES is similar apart from the treatment of the core-hole potential and projector $\mathcal{P}$.

A number of many-body effects can be incorporated in RTXS. For example, intrinsic losses from the dynamical response to the core-hole can be added subsequently *via* convolution with an additional broadening function given by the Fourier transform of the exponential $e^{C(t)}$, where the cumulant $C(t)$ can also be obtained from the transient Green's function.[1,12] Final state lifetime effects due to extrinsic processes and interference effects lead to additional damping, which here are crudely represented as an additional exponential decay factor $e^{-\gamma t}$. Note that the core-hole lifetime Γ as well as the decay of the correlation function serve as natural convergence factors in the calculation of the XAS, which limit the maximum time in the evaluation of Eq. (1). These effects will be considered in more detail in a subsequent paper.

To evaluate the time-correlation function, we use a fixed, local, nonorthogonal basis set $\phi_j(\vec{x}) \equiv |j\rangle$, as in the SIESTA code.[20] It is also convenient to define dual states $\langle\tilde{j}| = \Sigma_{j'} S^{-1}_{jj'}\langle j'|$, where $S_{jj'} = \langle j|j'\rangle$ is the overlap matrix. These states satisfy the orthogonality relations $\langle\tilde{j}|j'\rangle = \delta_{jj'}$, and are also well localized with respect to atomic sites to the extent the overlap matrix and its inverse are short ranged. In this local orbital orbital basis, the time-evolved state $|\psi(t)\rangle$ can be expanded as

$$|\psi(t)\rangle = \sum_j |j\rangle c_j(t). \tag{4}$$

At $t = 0$, the coefficients $c_j(0) = M_{jc}$ are given by quasilocal transition-matrix elements:

$$M_{jc} = \langle\tilde{j}|d|c\rangle = \sum_{j'} S^{-1}_{jj'}\langle j|d|c\rangle. \tag{5}$$

As noted above, the time evolution of $|\psi(t)\rangle$ can be expressed in terms of the unitary time-evolution operator $U(t,0)$ such that $|\psi(t)\rangle = U(t,0)|\psi(0)\rangle$, where

$$U(t,0) = T\exp\left[-i\int_0^t dt\,\mathbf{H}'(t)\right], \tag{6}$$

and T is the time-ordering operator. Thus the time-correlation function can be calculated directly using the transition-matrix elements and the local matrix elements of $\mathbf{U}$:

$$\langle\psi(0)|\psi(t)\rangle = \sum_{jj'}\langle c|d^\dagger|j\rangle U_{jj'}(t,0)\langle\tilde{j}'|d|c\rangle. \tag{7}$$

Calculations starting from $|\psi_+(0)\rangle$ or $|\psi_-(0)\rangle$ are similar, and make use of the same operator $U(t,0)$. Due to the local nature of the transition-matrix elements $\langle\tilde{j}|d|c\rangle$ for deep core-orbitals $|c\rangle$, the sums over orbitals in these basis-set expansions are limited to a small neighborhood of the core site. Moreover, since the final-state Hamiltonian is constant during the period of integration, the calculation of the time-evolution operator is highly efficient.

In our implementation for RTXS, the time evolution operator $U_{jj'}(t,t')$ is evaluated as a product over many small time-steps Δ using a Crank-Nicolson algorithm, i.e., $c_j(t+\Delta) = \sum_{j'} U_{jj'}(t+\Delta,t)c_{j'}(t)$, where (in matrix notation) the differential time-evolution operator is

$$\mathbf{U}(t+\Delta,t) = \frac{\mathbf{1} - i\mathbf{S}^{-1}\mathbf{H}'(\bar{t})\Delta/2}{\mathbf{1} + i\mathbf{S}^{-1}\mathbf{H}'(\bar{t})\Delta/2}, \tag{8}$$

and $\bar{t} = t + \Delta/2$. This approximation is manifestly unitary and also time reversible to second order in the time interval Δ, due to evaluating the operators at the interval midpoint $\bar{t}$. This prescription has been found to be stable for relatively long-time intervals Δ. $\mathbf{H}'(t)$ is the Hamiltonian of the final state evaluated in the local basis, which is independent of time over the region of integration. In XAS, a core hole is created during the photoelectron excitation while the remaining electrons relax to provide a screening charge. Thus, in addition to the Hartree Hamiltonian h_H and final-state self-energy Σ, $\mathbf{H}'(t)$ includes the screened core-hole potential $v_{\rm ch}$ with matrix elements $H'_{jj'} = \langle j|h_H + v_{\rm ch} + \Sigma|j'\rangle$.

In practice, the core-hole effect is introduced by substituting the neutral pseudopotential of the absorbing atom, with one that matches the full core-hole potential for the core-state $|c\rangle$. The system is then relaxed self-consistently in SIESTA in the presence of the core-hole. This produces, in a single initialization calculation, a Hartree Hamiltonian including the Coulomb potential obtained from the core-hole relaxed density, and a local pseudocharge. The resulting Hamiltonian is used for the subsequent propagation. For XES simulations, $v_{\rm ch}$ is not applicable, and the Hamiltonian matrix elements used are $H_{jj'} = \langle j|h_H + \Sigma|j'\rangle$. Although all matrix elements of $H'_{jj'}$ and $S_{jj'}$ are needed in the time evolution, only the local matrix elements $U_{jj'}(t,0)$ for j and j' in the neighborhood of the core-orbital are needed in the calculation of $\mu(\omega)$. In practical RTXS calculations, SIESTA is used only to obtain the

matrix elements of $\mathbf{H}'$ (or $\mathbf{H}$) and $\mathbf{S}$, the Fermi energy E_F and the basis functions $\phi_j(\vec{x})$ needed to construct the atomic matrix elements. The time-evolution operator matrix elements are calculated subsequently.

Physically, the Fourier transform of the time-correlation function can be interpreted as a local density of final, unoccupied electron states $\rho_+(\omega)$ defined for the state $|\psi_+\rangle$; i.e., the levels and amplitudes allowed by the transition operator in the presence of the core hole,

$$\rho_+(\omega) = \frac{1}{\pi \|\psi_+\|^2} \operatorname{Im} \int_0^\infty dt\, e^{i\omega t} \langle \psi_+(0)|\psi_+(t)\rangle, \quad (9)$$

where $\|\psi_+\|^2 \equiv \langle \psi_+(0)|\psi_+(0)\rangle$ is the normalization constant. For example, for K-shell absorption, the state $|\psi_+(0)\rangle$ is a superposition of local atomic-like p orbitals and $\rho_+(\omega)$ corresponds to the local final, unoccupied state p DOS, projected onto those orbitals. Similarly the density $\rho_-(\omega)$ corresponds to the density of occupied states of the initial-state Hamiltonian.

B. Equivalence to Fermi's golden rule

As noted in the introduction, the time-correlation approach discussed herein for dipole mediated transitions is equivalent to Fermi's golden rule within an effective independent particle picture and the ΔSCF approximation. To show this, one may evaluate the time correlation function formally in terms of the scattering eigenstates $|k'\rangle$ of H' calculated in the presence of a core hole. By expanding in one-particle states and applying the projector $\mathcal{P}$, we obtain the conventional sum-over-states expression for the golden rule in the independent particle approximation:

$$\mu(\omega) = \sum_{k'} |\langle c|d|k'\rangle|^2 \delta_\Gamma(E - \epsilon_{k'})\theta(E - E_F), \quad (10)$$

where $E = \omega + \epsilon_c$ and δ_Γ is a δ-like function of unit weight broadened by the core-hole lifetime Γ.

Alternatively one can demonstrate the equivalence from a spectral representation of the time-evolution operator. Given that the time-Fourier transform of $\mathbf{U}$ is proportional to the one-particle Green's function $G'(E)$ for the final state, [cf. Eq. (9)] calculated (for XAS) in the presence of a core-hole, the XAS from a core level at energy ϵ_c is

$$\mu(\omega) = -\frac{1}{\pi} \operatorname{Im} \langle c|d^\dagger \mathcal{P}\, G'(E)\, \mathcal{P} d|c\rangle, \quad (11)$$

which agrees with the formalism in the real-space Green's function (RSGF) approach used, e.g., in the FEFF codes.[21] Here, $G'(E) = [E - H' + i\Gamma]^{-1}$ is the retarded one-particle Green's function at energy $E = \omega + \epsilon_c$, H' is the one-electron Hamiltonian of the final quasiparticle state including a screened core hole and a final-state self-energy Σ, and again $\mathcal{P}$ is the projector onto unoccupied states above the Fermi energy. Finally, in the limiting case of an empty conduction band described by Wannier orbitals, this result for $\mu(\omega)$ reduces to

$$\mu(\omega) = |M_{0c}|^2 \rho'_{00}(E), \quad (12)$$

in agreement with Eq. (41) of Ref. 13. Here, $E = \epsilon_c + \omega$ and $\rho'_{00}(E)$ is the local density of states at the absorption site 0 in the presence of a core hole.

C. Local projection

In practice, it is computationally useful to simplify the above by projecting the initial state onto basis functions centered on the excited atom, when the initial state has a small overlap with other basis functions. For the systems studied in this paper, this produces good agreement with other theories and experiment as long as the projector is applied to the energy eigenvectors as well. Given a complete set of eigenvectors $\{|k\rangle\}$ with eigenvalues E_k so that $|k\rangle = \sum_j a_{kj}|j\rangle$, we may expand the seed state as

$$|\psi(0)\rangle = \sum_j c_j(0)|j\rangle = \sum_{k,ij} a^*_{ki} S_{ij} c_j(0)|k\rangle, \quad (13)$$

and the absorption/emission intensity for a given eigenvalue E_k as

$$W_k = |\langle k|\psi(0)\rangle|^2 = \sum_{ij} |a^*_{ki} S_{ij} c_j(0)|^2. \quad (14)$$

Due to the highly localized nature of the core states, the seed state can be approximated as a local initial state $\mathcal{P}_A|\psi(0)\rangle$, where $\mathcal{P}_A$ projects onto the subset of basis set vectors centered on the excited atom A,

$$\mathcal{P}_A = \sum_{i\in A} |i\rangle\langle\tilde{i}|. \quad (15)$$

Within this approximation, the local spectral weight is

$$W^A_k = |\langle k|\mathcal{P}^\dagger_A \mathcal{P}_A|\psi(0)\rangle|^2 = \sum_{ij\in A} |a^*_{ki} S_{ij} c_j(0)|^2, \quad (16)$$

and the time-correlation function $C(t) = \langle\psi(0)|\psi(t)\rangle$ can be approximated as a local quantity:

$$C_A(t) = \langle \psi_A(0)|\psi_A(t)\rangle, \quad (17)$$

where

$$|\psi_A(t)\rangle = \mathbf{U}(t,0)\mathcal{P}^\dagger_A \mathcal{P}_A|\psi(0)\rangle. \quad (18)$$

Although this simplification provides only minor performance improvements, it highlights the local nature of the process where a photoelectron state is created.

D. Transition matrix elements

To obtain the seed state for the time correlation formalism, we must first compute the transition matrix elements M_{jc} in Eq. (5). These matrix elements involve a core state $|c\rangle$, a local basis function $|j\rangle$, and the dipole interaction $d(x)$ (in position representation). Since the SIESTA $|j\rangle$ basis functions are atomic orbitals of the pseudoatom, the core regions must be reconstructed to find the correct matrix elements.[22,23] For this purpose we use the projector augmented wave (PAW) engine from the core-level spectroscopy code OCEAN.[24]

Given an arbitrary all-electron wave function $|\psi_{\text{ae}}\rangle$ and its associated pseudowave $|\psi_{\text{ps}}\rangle$, the PAW reconstruction transformation operator $\mathcal{T}$ is defined as

$$|\psi_{\text{ae}}\rangle = \mathcal{T}|\psi_{\text{ps}}\rangle. \quad (19)$$

Thus the pseudowave $\{|\phi^i_{\text{ps}}\rangle\}$ and all-electron basis orbitals $\{|\phi^i_{\text{ae}}\rangle\}$ satisfy the relation

$$|\phi^i_{\text{ae}}\rangle = \mathcal{T}|\phi^i_{\text{ps}}\rangle. \quad (20)$$

We may therefore define a projector basis set $\{\langle p^i|\}$ that satisfies $\langle p^i|\phi^j_{\rm ps}\rangle = \delta_{ij}$ inside some cutoff r_c, to be specified below; $\{|\phi^i_{\rm ps}\rangle\}$, $\{|\phi^i_{\rm ae}\rangle\}$, and $\{\langle p^i|\}$ are set to zero outside r_c. This cutoff is chosen so that it satisfies OCEAN's requirement that it be large enough that the pseudo- and all-electron wave functions agree beyond it. Furthermore, we require r_c to be greater than the SIESTA pseudo-wave-function cutoff, beyond which the basis functions are set to zero.

The PAW reconstruction operator is given formally by

$$\mathcal{T} = 1 + \left(|\phi^i_{\rm ae}\rangle - |\phi^i_{\rm ps}\rangle\right)\langle p^i|. \tag{21}$$

Since $|c\rangle$ is well localized within r_c, the reconstruction operator simplifies to $\mathcal{T} = |\phi^i_{\rm ae}\rangle\langle p^i|$. Then the matrix elements may be expressed as $\langle\tilde{i}|\mathcal{T}^\dagger d|c\rangle$, resulting in the following expression for the seed state:

$$|\psi_{\rm ps}(0)\rangle = \sum_{i,j} |i\rangle\langle\tilde{i}|p^j\rangle\langle\phi^j_{\rm ae}|d|c\rangle. \tag{22}$$

It should be noted that the calculation of $\langle\tilde{i}|p^j\rangle$ is possible because we choose r_c greater than the $|i\rangle$ cutoff. Moreover, the core reconstruction calculation for XAS is done without a core hole, consistent with the approach described in Sec. II A.

III. COMPUTATIONAL DETAILS

A. Model systems

To demonstrate the versatility of the RTXS time-correlation approach, we present illustrative calculations for three representative systems: benzene (C_6H_6), trinitrotoluene (TNT, $C_7H_5N_3O_6$) and diamond. Benzene (see Fig. 1) is simulated in its gas phase conformation.[25] For TNT we use one of the symmetry-inequivalent molecules in its crystalline structure (see Fig. 2).[26] We have previously shown[27] that this yields well converged results compared to experiment. Diamond is modeled using a $C_{47}H_{60}$ hydrogen-capped cluster, shown in Fig. 3, generated using the experimental lattice constant of 3.5668 Å and including five carbon shells around a central absorber. For comparison, diamond calculations were also performed using periodic boundary conditions (PBC) on a $2 \times 2 \times 2$ supercell of the conventional eight-atom orthogonal cell with the same lattice constant.

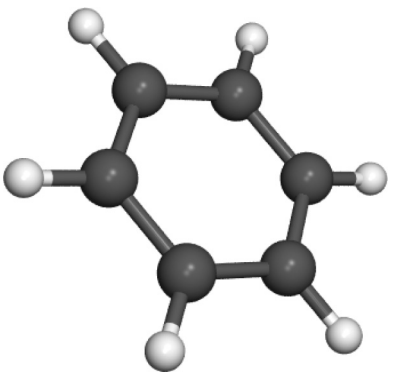

FIG. 1. Gas phase structure of benzene (C_6H_6) used in the RTXS and StoBe simulations,[25] where C is dark gray and H is white.

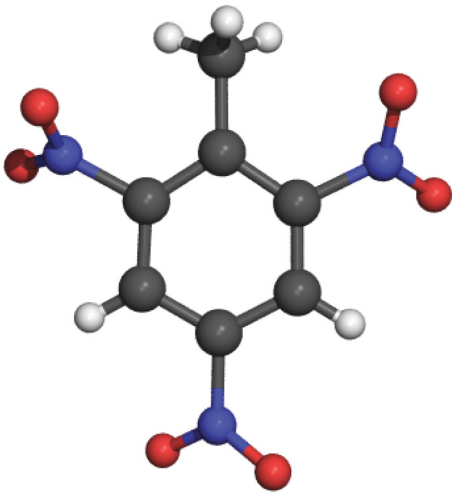

FIG. 2. (Color online) Crystalline structure of a single symmetry-inequivalent molecule of trinitrotoluene (TNT, $C_7H_5N_3O_6$) used in the RTXS, StoBe, and FEFF simulations, where C is dark gray, H is white, O is red (light gray), and N is blue (medium gray).

B. RTXS

The RTXS calculations use a SIESTA triple-ζ basis set with two d-polarization functions on the C, N, and O atoms and two p-polarization functions on the H atoms (TZDP). The cutoff radii are set using an energy shift[20] of 1 meV, which results in typical cutoffs of about 5 to 10 Bohr. The SIESTA calculations also use an auxiliary real-space grid with an equivalent plane-wave cutoff of 150 Ry. This choice of polarization functions and cutoff radii ensures a good representation of all the valence occupied states as well as the valence unoccupied states up to about 30 eV above threshold. For consistency with the StoBe simulations described below, all RTXS simulations used the PBE[28] exchange-correlation functional. Typical total RTXS simulations were carried out to $t_{\rm max} = 5$–15 fs, long enough that modes with frequencies above 0.5–1 eV do not

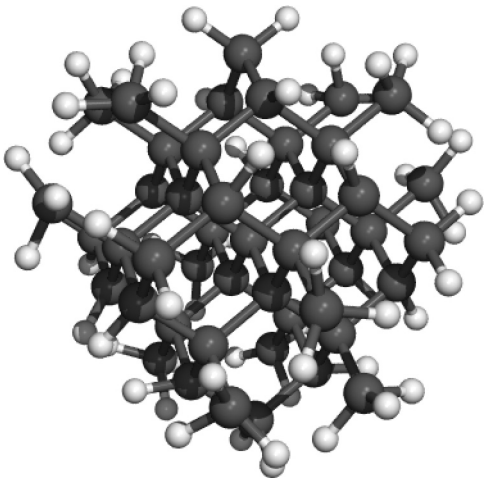

FIG. 3. Structure of the hydrogen-capped diamond cluster ($C_{47}H_{60}$) used in the RTXS, StoBe, and FEFF simulations, where C is dark gray and H is white. The cluster is generated using the experimental structure of diamond with lattice constant 3.5668 Å, and includes five carbon shells around the absorber.

appear as nonperiodic trends. The typical time steps were 0.01 fs, which accommodate frequencies as high as 50 eV. The final spectra are shifted to fit experimental peak positions and broadened to match the experimental broadening. To do this, first, an exponential damping is added to the raw correlation such that the correlation is below 0.01 at the end of the time series; this yields an initial Lorentzian broadening. Second, Gaussian broadening is added to the Fourier transformed spectra to match experimental broadening. For XAS, the Gaussian broadening has a standard deviation $\sigma(E)$, which varies with energy:

$$\sigma(E) = \begin{cases} \sigma_{\min}, & E < E_1, \\ \sigma_{\min} + \gamma(E - E_1), & E_1 \leqslant E \leqslant E_2, \\ \sigma_{\min} + \gamma(E_2 - E_1), & E > E_2, \end{cases} \quad (23)$$

where $\sigma_{\min}$, E_1, E_2, and γ depend on the system. For XES, the Gaussian broadening is constant. This approach is analogous to that implemented in StoBe.[6,29]

We use nonrelativistic, kinetic-energy optimized, norm-conserving pseudopotentials, with and without a core hole. These are generated with OPIUM,[30] using the PBE exchange-correlation functional. The neutral and core-hole pseudopotential cutoff radii are equal, except as needed by the introduction of the core hole. In the systems simulated here, only C and N atoms are excited. For the N pseudopotential, the reference configuration is $1s^2 2s^2 2p^3$ and for C it is $1s^2 2s^2 2p^2$ or $1s^1 2s^2 2p^2$, depending on the presence of a core hole. For carbon without a core hole, the core cutoff radii are 1.40 Bohr for all l channels. For carbon with a core hole, the cutoff radii are 1.25 Bohr for all l channels, except the $2p$ states, which have a cutoff radius of 1.20 Bohr. For nitrogen without a core hole, the cutoff radii are 1.25 Bohr for all l channels.

C. StoBe

For comparison, StoBe-deMon simulations were carried out using the IGLO-III[31] basis set for the absorbing atoms, while the (311/211) ECP StoBe basis set[32] was used for all other atoms except H which used the 6–311 + G set.[33] The Coulomb and exchange correlation potentials were fitted and expanded over auxiliary basis sets with (NC(s), NC(spd); NXC(s), NXC(spd)) s and spd-type functions. Auxiliary sets of (5,2;5,2) quality were used for the C, N, and O atoms, and of (3,1;3,1) quality for the H atoms. All StoBe-deMon calculations used the PBE[28] exchange-correlation functional. The XAS[6] and XES[29] StoBe-deMon calculations use the "frozen-orbital" approximation with Kohn-Sham single-particle orbitals. While the XES simulations use ground-state orbitals, XAS results were obtained using the transition potential approximation, a simplification of the Slater's transition state core-hole approximation, in which the core spin orbital is populated with half an electron and the excited half electron is neglected. This allows obtaining all excited states from one diagonalization. In contrast, it should be noted that the RTXS simulations use a full self-consistently screened core hole. For comparison, we also performed test StoBe calculations using a full core hole. For the systems studied here we find that, apart from an energy shift, the half core-hole and full core-hole spectra are quite similar.

D. FEFF

Additional comparisons were carried out using version 9 of the FEFF code.[21] This approach is based on the RSGF formalism, which includes approximate calculations of many-body effects including inelastic losses and Debye-Waller factors. For XAS, the final state is calculated in the presence of a statically screened core hole, i.e., the final state rule (FSR); for XES the calculations are done without a core hole. In many respects, the RSGF approach in FEFF is the frequency-space analog of the RTXS approach discussed in this paper. FEFF uses a basis of relativistic, angular-momentum scattering states $|L,\mathbf{R}\rangle$ to describe electronic states. Therefore it is expected to be more accurate than either RTXS and StoBe at energies high above the edge. However, FEFF's use of spherical muffin-tin potentials makes the code less accurate near the edge. The core-hole potential is obtained using a self-consistent Dirac-Fock calculation for an atom with an atomic configuration containing a hole in a given level, e.g., $1s$ for the K-shell calculations presented here. Here, we have used the FEFF9 code with 5-Å clusters for the generation of the

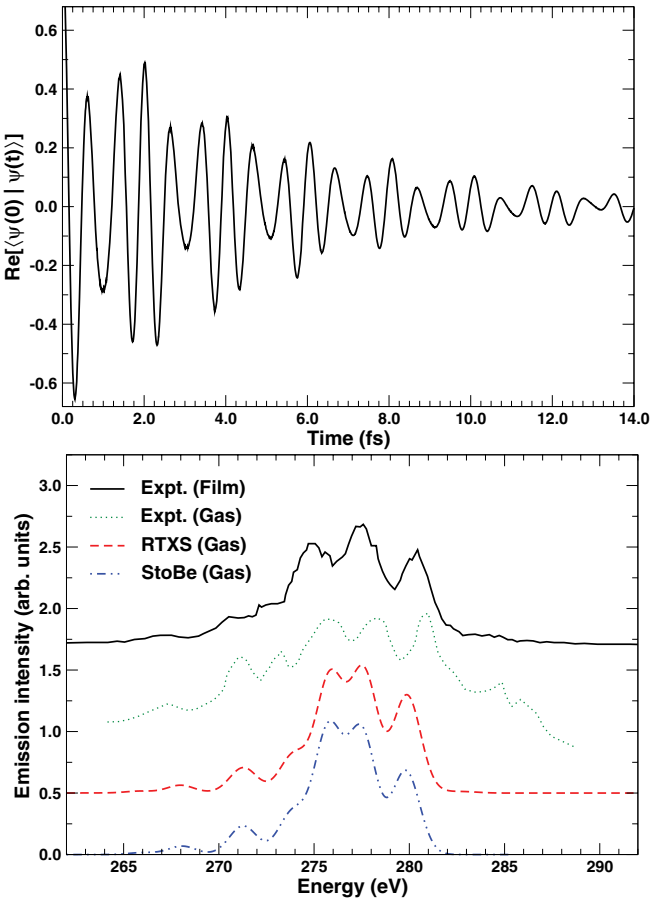

FIG. 4. (Color online) (Top) Real part of the Fourier filtered RTXS time correlation function for the C K-edge XES of benzene. (Bottom) Real-time (RTXS, corresponding to the time correlation function shown above) and StoBe simulations of the C K_α XES of benzene gas (C_6H_6) compared to experiment in film[34] and gas phase[35] conditions. The gas phase measurement corresponds to electron rather than photon excitation.

self-consistent muffin-tin potentials and 9-Å clusters for the calculations of the full multiple scattering XAS (or XES).

IV. RESULTS

A. Benzene

Given its structural and electronic simplicity, benzene is a good system to test our approach. The XES autocorrelation function, shown in Fig. 4, has a relatively simple structure involving a few timescales. The associated spectrum (also in Fig. 4), is dominated by three high intensity peaks 4, 6, and 8 eV below threshold, and three low-intensity ones at lower energies. The width σ is set to 0.7 eV and the spectrum is shifted by 286.0 eV to match experiment. The high intensity peaks are associated with clearly visible 0.4–0.6 fs periods in the autocorrelation function, and are due to emission from orbitals with symmetry $1e_{1g}$ (279.8 eV), $3e_{2g}$ (277.5 eV), and $1b_{2u}/3e_{1u}$ (276.0 eV).

For comparison, Fig. 4 also shows experimental and StoBe results. The agreement with StoBe is quite good and serves as a validation of our methodology. The most noticeable difference arises for the two most intense peaks. The small difference in intensity ratio is due mostly to the projection onto local basis orbitals from the initial state. Both RTXS and StoBe calculations show good overall agreement with experiment, and slightly underestimate the splittings in the triplet of intense peaks.

B. Trinitrotoluene

Trinitrotoluene (TNT) poses a more significant challenge to the theory due to its complex electronic structure and multiple absorbing N atoms.[27] As for C_6H_6, we find very good agreement between RTXS and StoBe (see Fig. 5). For RTXS, σ was set to 2.0 eV and the spectrum shifted by 407.0 eV to match the K-shell experiment. Moreover, we also find fairly good agreement with the RSGF approach in FEFF; however, the discrepancies are likely due to the use of spherical muffin-tin potentials in FEFF. As discussed in Ref. 27, the lower intensity with respect to experiment in the 385–390 eV region is due to an underestimation of the transition intensities associated with σ_{NC} bonds. In general, intensities associated with σ bonds are more affected by vibrational distortions (not included in our simulations) than π bonds.

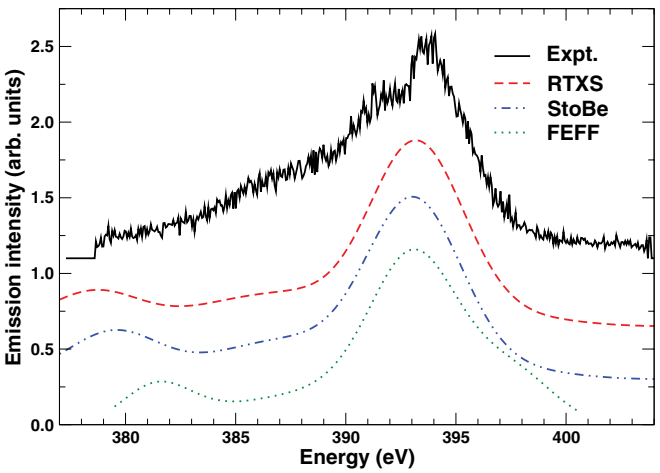

FIG. 5. (Color online) Real-time (RTXS), StoBe, and FEFF simulations of the N K_α XES of trinitrotoluene (TNT, $C_7H_5N_3O_6$) compared to experiment measured in a film.[27]

C. Diamond

As a third example we present results for diamond, a relatively simple yet challenging insulating crystalline solid. Figure 6 shows the RTXS XES results in comparison with StoBe calculations and experimental measurement. For RTXS, σ was set to 1.9 eV and the spectrum is shifted by 285.6 eV to match experiment. As in the previous examples, the agreement between RTXS and StoBe is fairly good despite the slightly different broadening schemes. The RTXS results are also in very good agreement with experiment, accounting for the broad 275–283 eV feature, and the small peak at 270 eV. In RTXS, the broad feature is composed of two peaks at 279.8 and 276.9 eV, with almost equal intensity, and a less intense peak at 274.7 eV. The two latter peaks form the broad shoulder at about 275 eV. The overall width of this feature, about 7.9 eV, corresponds to the occupied valence bandwidth and is in good

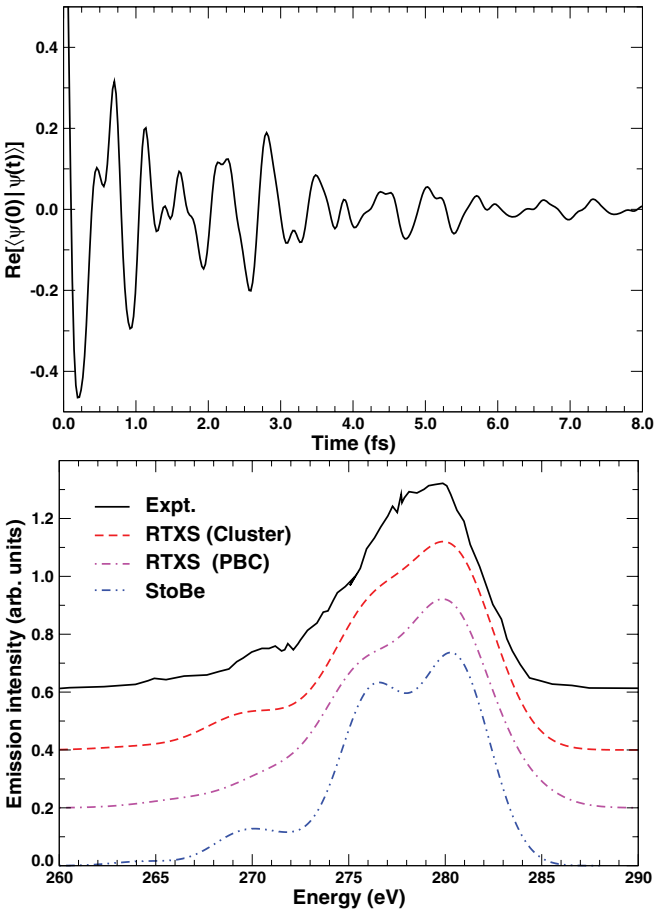

FIG. 6. (Color online) (Top) Real part of the Fourier filtered RTXS time correlation function for the C K-edge XES of diamond (simulated using a $C_{47}H_{60}$ cluster). (Bottom) Real-time (RTXS, corresponding to the time correlation function shown above) and StoBe simulations of the C K_α XES of diamond compared to experiment.[36] The RTXS calculations used either a $C_{47}H_{60}$ cluster or a $2 \times 2 \times 2$ supercell of the conventional eight-atom orthogonal cell with periodic boundary conditions (PBC).

agreement with the experimental width of 7.2 eV. The broad feature at 270 eV is composed of several low intensity peaks. Figure 6 also shows the real-time autocorrelation function associated with the RTXS XES. Given the number of states involved in the XES, it is not surprising that the correlation function is quite complex, exhibiting a variety of timescales. Most noticeable are periods of about 0.5 and 0.4 fs, associated with the broad 275–283 eV feature, overlaid with shorter (about 0.2 fs) oscillations associated with the broad feature at 270 eV.

Our RTXS implementation is currently able to compute XES spectra using periodic boundary conditions (PBC), i.e., with the initial-state Hamiltonian without a core hole. Figure 6 shows a comparison between the $C_{47}H_{60}$ cluster model and PBC model, where the PBC calculation used a $2 \times 2 \times 2$ supercell of the conventional eight-atom orthogonal cell. Both methods give similar results, with the cluster approach being closer to experiment, in particular in the 270 eV region.

Figure 7 presents the XAS spectra of diamond computed with RTXS, StoBe, and FEFF, compared to experiment. The RTXS spectra uses broadening parameters $\sigma_{\min} = 0.8$ eV, $E_1 = 297.9$ eV, $E_2 = 302.9$ eV, and $\gamma = 0.4$ eV, using the notation in Eq. (23), and a shift of 285.7 eV to match the energies of the experimental peaks. In the near-edge region (285–310 eV), RTXS is in very good agreement with experiment, showing better splittings and relative intensities at 292 and 298 eV than either FEFF and StoBe. RTXS also shows very good agreement in the overall width of the unoccupied valence band, with a predicted width of 11 eV versus 11.5 eV observed in the experiment. In the edge region, FEFF has limitations originating from the use of spherical potentials that hinder its ability to represent highly directional bonds. At higher energies (i.e., above 310 eV), RTXS yields worse agreement than either FEFF or StoBe. This is likely due to the limitations in the local basis sets—local numerical atomic orbitals for SIESTA and Gaussian-type orbitals for StoBe—which only provide a limited representation of the delocalized states in the continuum. Exploratory calculations show that with the present basis set, RTXS results begin to exhibit variations due to the quality of the basis set 30 eV above threshold. On the other hand FEFF provides the broadest overall agreement with experiment due to the superior performance of the RSGF approach at high energies. Figure 7 also shows the associated autocorrelation function, which is significantly more complicated than the XES one. Given that the spectrum is composed of a large number of states, it is difficult to observe any dominant timescales.

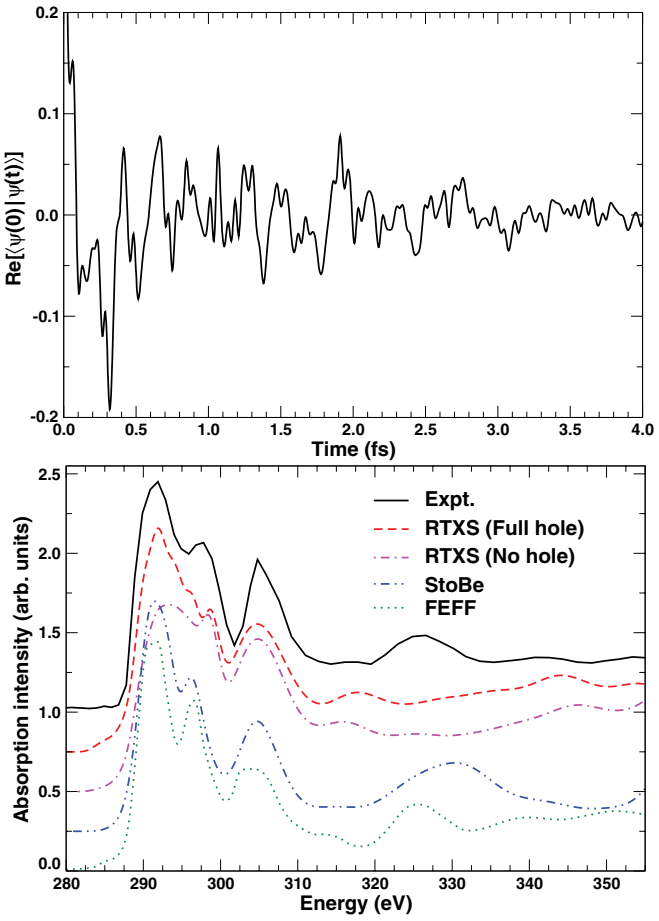

FIG. 7. (Color online) (Top) Real part of the Fourier filtered RTXS time correlation function for the C K-edge XAS of diamond (simulated using a $C_{47}H_{60}$ cluster). (Bottom) Real-time (RTXS, corresponding to the time correlation function shown above), StoBe, and FEFF simulations of this system vs experiment.[37] The RTXS XAS is calculated with and without a core hole, while StoBe uses a half core-hole prescription.

As described in Sec. II A, XAS spectra present an additional challenge with respect to XES in that an adequate treatment of the screened core-hole is required. In addition, it appears that the treatment of core-hole screening is responsible for much of the difference in diamond absorption spectra between StoBe and RTXS. Therefore it is interesting to explore the effect of ignoring the core-hole in the RTXS calculations. As shown in Fig. 7, we find that the core hole has a noticeable effect near the edge, increasing the intensity and narrowing the width of the feature associated with the σ bonds at 292 eV. This reflects the large charge density relaxation and consequent excitonic enhancement induced by the attractive core-hole potential on the bond network surrounding the absorber. At present, our RTXS implementation is limited to the no core-hole or fully screened (i.e., with SCF-DFT screening) core-hole approximations. More flexible core-hole treatments, e.g., using partial core charging, would allow better comparisons with other methods such as the half core hole used in StoBe.

V. CONCLUSIONS

We have introduced a real-time approach (RTXS) for the calculation of XAS and XES based on time-correlation functions. The approach is equivalent to ΔSCF Fermi's golden rule calculations. The spectra are calculated from the Fourier transform of the autocorrelation function of the time-evolving wave function, together with the core-hole Green's function. The method is implemented as an extension of our real-time time-dependent density functional SIESTA code, and includes PAW transition matrix elements. We have compared RTXS calculations of XAS and XES with spectra from experiment, StoBe and FEFF. RTXS and StoBe produce similar emission spectra, with RTXS slightly closer to experiment in the case of

diamond. In contrast, notable differences are found between RTXS and StoBe for XAS. In the case of diamond, RTXS models the near-edge XAS region more realistically than either FEFF or StoBe. The improvement compared to FEFF is likely due to the inclusion of nonspherical potentials, while differences with StoBe are probably due to the treatment of core-hole screening.

ACKNOWLEDGMENTS

We thank G. Bertsch, J. Kas, R. Markiewicz, D. Prendergast, A. Rubio, R. Santra, and J. T. Vinson for discussions and insights. This work was initiated at a KITP program on x-ray Frontiers and was supported in part by NSF CDI Grant PHY-0835543.

[1]P. Nozières and C. T. De Dominicis, Phys. Rev. **178**, 1097 (1969).
[2]J. J. Rehr and R. Alben, Phys. Rev. B **16**, 2400 (1977).
[3]Y. Takimoto, F. D. Vila, and J. J. Rehr, J. Chem. Phys. **127**, 154114 (2007).
[4]F. D. Vila, J. J. Rehr, H. H. Rossner, and H. J. Krappe, Phys. Rev. B **76**, 014301 (2007).
[5]M. Taillefumier, D. Cabaret, A.-M. Flank, and F. Mauri, Phys. Rev. B **66**, 195107 (2002).
[6]L. Triguero, L. G. M. Pettersson, and H. Ågren, Phys. Rev. B **58**, 8097 (1998).
[7]H. Ebert, Rep. Prog. Phys. **59**, 1665 (1996).
[8]M. Ljungberg, J. Mortensen, and L. Pettersson, J. Electron Spectrosc. Relat. Phenom. **184**, 427 (2011).
[9]L. Young *et al*., Nature (London) **466**, 56 (2010).
[10]K. Yabana and G. F. Bertsch, Phys. Rev. B **54**, 4484 (1996).
[11]G. F. Bertsch, J.-I. Iwata, A. Rubio, and K. Yabana, Phys. Rev. B **62**, 7998 (2000).
[12]D. C. Langreth, Phys. Rev. B **1**, 471 (1970).
[13]V. I. Grebennikov, Y. A. Babanov, and O. B. Sokolov, Phys. Status Solidi B **79**, 423 (1977).
[14]O. Wessely, O. Eriksson, and M. I. Katsnelson, Phys. Rev. B **73**, 075402 (2006).
[15]T. Privalov, F. Gel'mukhanov, and H. Ågren, Phys. Rev. B **64**, 165115 (2001).
[16]U. von Barth and G. Grossmann, Phys. Rev. B **25**, 5150 (1982).
[17]J. J. Rehr and R. C. Albers, Rev. Mod. Phys. **72**, 621 (2000).
[18]J. Crank and P. Nicolson, Math. Proc. Cambridge **43**, 50 (1947).
[19]P. E. Blöchl, Phys. Rev. B **50**, 17953 (1994).
[20]J. M. Soler, E. Artacho, J. D. Gale, A. García, J. Junquera, P. Ordejón, and D. Sánchez-Portal, J. Phys.: Condens. Matter **14**, 2745 (2002).
[21]J. J. Rehr, J. J. Kas, M. P. Prange, A. P. Sorini, Y. Takimoto, and F. Vila, C. R. Phys. **10**, 548 (2009).
[22]P. E. Blochl, Phys. Rev. B **41**, 5414 (1990).
[23]B. Hetenyi, J. Phys. Chem. **120**, 8632 (2004).
[24]J. Vinson, J. J. Rehr, J. J. Kas, and E. L. Shirley, Phys. Rev. B **83**, 115106 (2011).
[25]G. Herzberg, *Electronic Spectra and Electronic Structure of Polyatomic Molecules* (Van Nostrand, New York, 1966).
[26]W. R. Carper, L. P. Davis, and M. W. Extine, J. Phys. Chem. **86**, 459 (1982).
[27]F. D. Vila, T. Jach, W. T. Elam, J. J. Rehr, and J. D. Denlinger, J. Phys. Chem. A **115**, 3243 (2011).
[28]J. P. Perdew, K. Burke, and M. Ernzerhof, Phys. Rev. Lett. **77**, 3865 (1996).
[29]L. Triguero, L. Pettersson, and H. Ågren, J. Phys. Chem. A **102**, 10599 (1998).
[30]A. M. Rappe, K. M. Rabe, E. Kaxiras, and J. D. Joannopoulos, Phys. Rev. B **41**, 1227 (1990).
[31]W. Kutzelnigg, U. Fleischer, and M. Schindler, in *The IGLO-Method: Ab Initio Calculation and Interpretation of NMR Chemical Shifts and Magnetic Susceptibilities*, Vol. 23 (Springer-Verlag, Heidelberg, 1990).
[32]L. Pettersson (unpublished).
[33]R. Krishnan, J. S. Binkley, R. Seeger, and J. A. Pople, J. Chem. Phys. **72**, 650 (1980).
[34]P. Skytt, J. Guo, N. Wassdahl, J. Nordgren, Y. Luo, and H. Ågren, Phys. Rev. A **52**, 3572 (1995).
[35]J. Nordgren, L. Selander, L. Pettersson, R. Brammer, M. Bäckström, C. Nordling, and H. Ågren, Phys. Scr. **27**, 169 (1983).
[36]Y. Ma, N. Wassdahl, P. Skytt, J. Guo, J. Nordgren, P. D. Johnson, J.-E. Rubensson, T. Boske, W. Eberhardt, and S. D. Kevan, Phys. Rev. Lett. **69**, 2598 (1992).
[37]T. T. Fister, G. T. Seidler, J. J. Rehr, J. J. Kas, W. T. Elam, J. O. Cross, and K. P. Nagle, Phys. Rev. B **75**, 174106 (2007).